Vehicle Localization During GPS Outages With Extended Kalman Filter and Deep Learning

Jiageng Liu and Ge Guo, *Senior Member, IEEE*

***Abstract*— Integration of microelectromechanical system-based inertial navigation system (MEMS-INS) and global positioning system (GPS) is a promising approach to vehicle localization. However, such a scheme may have poor performance during GPS outages and is less robust to measurement noises in changeable urban environments. In this article, we give an improved extended Kalman filter (IEKF) using an adaptation mechanism to eliminate the influence of noises in MEMS-INS and mitigate dependence on the process model. Especially, to guarantee accurate position estimation of the INS, a deep learning framework with multiple long short-term memory (multi-LSTM) modules is proposed to predict the increment of the vehicle position based on Gaussian mixture model (GMM) and Kullback–Leibler (KL) distance. The IEKF and the multi-LSTM are then combined together to optimize vehicle positioning accuracy during GPS outages in changeable urban environments. Numerical simulations and real-world experiments have demonstrated the effectiveness of the combined IEKF and multi-LSTM method, with the root-mean-square error (RMSE) of predicted position reduced by up to 93.9%. Or specifically, the RMSEs during GPS outages with durations 30, 60, and 120 s are 2.34, 2.69, and 3.08 m, respectively, which obviously outperform the existing method.**

***Index Terms*— Deep learning, global positioning system (GPS) outages, improved extended Kalman filter (IEKF), prediction, vehicle localization.**

I. Introduction

REAL-TIME, accurate, robust positioning is very important for vehicular and intelligent transportation system (ITS) applications [1], [2]. There are many vehicle localization technologies for urban environments using various sensors such as RADAR, LiDAR, ultrasonic, HD maps, inertial sensors, and cameras [1]–[3]. The most popular is the global positioning system (GPS), which can provide accurate position and velocity information when the signal is stable and continuous [4]–[8]. However, its update frequency (10 Hz) and positioning accuracy (4.9 m) are low [9] and suffers from poor signals or outages in situations with blockage and multipath [4], in forests, tunnels [3], and near buildings [7]. The 5G networks may improve GPS technology in terms of accuracy, real-time capability, and usability. However, 5G networks require more expensive base stations and have multiple bands that may yield adverse impact. Therefore, it is important to find a proper vehicle localization method to implement real-time accurate positioning during GPS outages in certain urban environments.

One can improve vehicle localization system using LiDAR-based or high-precision map-based technologies. A less expensive alternative is to integrate inertial navigation systems (INSs) and GPS to provide accurate and continuous position information [10]. Recently, some novel attempts have been conducted to improve the performance of INS/GPS. Among them, the most popular ones are enhancement of conventional INS/GPS, e.g., replacing the conventional INS with a microelectromechanical system (MEMS-INS) [5], [8], [11]. However, such a scheme may have larger accumulative errors [11], [12] and highly uncertain noises [13]. In particular, when GPS signals are blocked, it operates as a pure MEMS-INS [14], which implies significantly decreased accuracy, especially for long-term positioning [4]. For this reason, great research effort has been made to find methods to mitigate the weakness of integrated MEMS-INS/GPS so as to have stable position information during GPS outages.

One strategy is to provide external observation by adding additional sensors such as odometers [9], map data, wheel-speed sensors, and steering sensors [4]. This solution relies on additional auxiliary sensors and is costly [15]. Another method is to use time series prediction to update some of the measurements [16]. For instance, one can utilize Allan variance analysis [13] or autoregressive processes [4] to deal with the noise in MEMS sensors. The method based on time series is ineffective when GPS signals disappear for a long time. Some fusion algorithms are also derived using Kalman filter and its variants such as extended Kalman filter (EKF), unscented Kalman Filter (UKF), and cubature Kalman filter (CKF) [15]. However, it is rather hard to determine the accelerometer deviation and the gyro drift due to highly uncertain noise in MEMS-INS, and most of the current fusion algorithms are overly dependent on the preestablish process model. Recently, artificial intelligence (AI)-based models have been proposed to compensate for MEMS-INS errors during GPS outages [17]–[25]. When GPS signal is unavailable, the AI model can predict GPS pseudo increment via online learning [26]. Since the noise characteristics of MEMS-INS in the prediction stage might be different from the training stage [27], such a compensation may be inappropriate and degrade the performance.

Manuscript received May 21, 2021; accepted June 30, 2021. Date of publication July 15, 2021; date of current version July 19, 2021. This work was supported in part by the National Natural Science Foundation of China under Grant 61573077 and Grant U1808205. The Associate Editor coordinating the review process was Dr. Zhengyu Peng. *(Corresponding author: Ge Guo.)*

Jiageng Liu is with the College of Information Science and Engineering, Northeastern University, Shenyang 110819, China (e-mail: liu331453318@163.com).

Ge Guo is with the State Key Laboratory of Synthetical Automation for Process Industries, Northeastern University, Shenyang 110819, China (e-mail: geguo@yeah.net).

Digital Object Identifier 10.1109/TIM.2021.3097401

It is worth noting that the existing methods merely focus on the correlation between the increment of GPS pseudo signal and MEMS-INS errors. Unfortunately, the errors of MEMS-INS are not resulted from the GPS signal [21], [28], [29]. Therefore, the correlation can only meet the requirement when the conditions are invariable. Under varying conditions, this may lead to a false description of MEMS-INS errors. Meanwhile, the frequency of GPS signals (10 Hz) and MEMS-INS (100 Hz) is often difficult to synchronize with each other. This means that the input and output of the AI models need time alignment before training, which is difficult to achieve.

Therefore, to obtain accurate estimates, this article gives an improved extended Kalman filter (IEKF) for fusion of MEMS-INS and GPS signals to achieve accurate position estimation. Then, a deep learning model based on multiple long short-term memory (multi-LSTM) is introduced to predict the increment of the vehicle position during GPS outages. The combination of IEKF and multi-LSTM can enhance the position estimation with guaranteed accuracy and stability in various environments, which has been shown by simulations and real road experimental results. The main contributions of this article are summarized as follows.

1) An adaptation mechanism is introduced into the filter based on the error of the estimated state to address issues such as process model drift. The enhanced EKF is capable of handling inherent nonlinearities in the measurements and state, making it more accurate, fault tolerant, and independent of the process model.
2) In comparison with the existing models, the training method here is based on a new objective function which is built on the corrected position increment. With this training method, the vehicle positioning accuracy during GPS outages can be improved without additional data alignment algorithm.
3) A traffic condition classification algorithm is given based on the Gaussian mixture model (GMM) and Kullback–Leibler (KL) distance, which dictates which of the multi-LSTM modules should be active. In this way, the positioning accuracy can be improved for vehicles in changeable urban environments during GPS outages.

The remainder of this article is organized as follows. Section II gives the overview of the proposed methodology. The system setting and modeling are presented in Section III. Verification simulations and experimental results are given in Section IV. Section V gives the conclusion and future work.

II. Overview of the Proposed Methodology

The vehicle self-localization system is based on integration of sensors including MEMS-INS, GPS, wheel speed sensor, steering angle sensor, and on-board cameras. The wheel speed sensor and steering angle sensor provide longitudinal velocity and lateral velocity, respectively, while the on-board cameras take the role of monitoring or estimating the state of traffic scenes on a regular time basis. More specifically, under different traffic scenes (e.g., light traffic, medium traffic, and heavy traffic) in urban road environments, the vehicle experiences

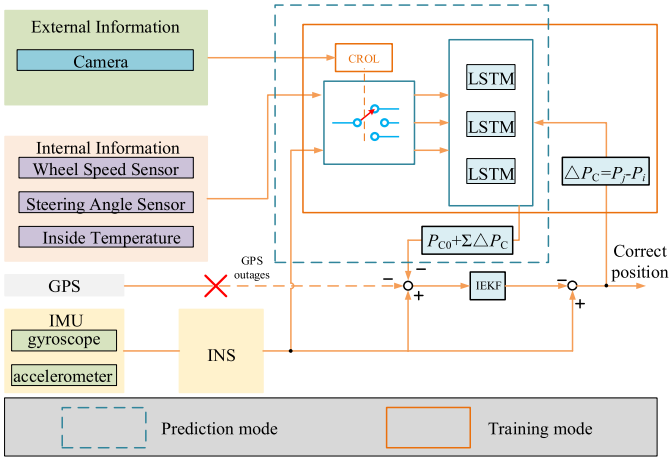

Fig. 1. Structure of the localization methodology. Here, P_i and P_j are the real position at instants i and j ($j = i + d$, where d is the time step of the training model), ΔP_C is the position increment, and P_{C0} is the initial position when GPS is unavailable.

different driving modes such as smooth, stop-and-go, and so on. This can lead to differences in not only the measurement noises of INS sensors but also the features of the camera output. Here, we use complexity levels (e.g., low, medium, and high) to indicate different traffic scenes.

The overall structure of the localization framework is shown in Fig. 1, which comprises an IEKF module and a position increment predictor based on a multi-LSTM model. The IEKF module plays the role of integrating the data of the inertial measurement unit (IMU) and GPS. It operates in two steps, in which the first step is to calculate the state estimation and then adjust the weight of the observed parameters of the system state via an adaptive adjustment factor. The second step is to modify the measurement update and then calculate the error correction and state prediction. The IEKF can achieve a relatively accurate position and reduce the influence on the estimate of the uncertain MEMS-INS noise.

The position increment predictor has two components, i.e., an external information detection model and a multi-LSTM model. The environment detection model is responsible for evaluating the traffic conditions according to the camera input (low-, medium-, and high-level complexity). Based on the evaluation, the model can choose different LSTM models corresponding to the complexity levels. The multi-LSTM model is composed of three LSTM modules, each of which has an independent learning strategy. The input of the architecture is the vehicle operating environmental states (both internal and external states). The internal environment variables include the wheel speed, steering angle, angular rate, specific force, and temperature inside of IMU. The external environment state covers the information from the camera. The output of the architecture is the estimated position increment information.

The localization system operates in two modes, e.g., training mode and prediction mode, depending on whether the GPS signal is available or not. The system can autonomously select the adaptive LSTM models for prediction based on the camera input and then output the predicted position increment

information. The predicted value is accumulated with the initial correct position information and then yields the position estimate through the IEKF.

III. Development of the Method

A. MEMS-INS Error Model

The MEMS-INS uses accelerometer and rate gyroscope to provide position, velocity, and attitude information. According to [21], the errors of rate gyros and accelerometer, due to bias, thermo-mechanical white noise, flicker noise, and temperature effect, are described in (1) and (2), respectively

$$\begin{cases} \theta_C(t) = \varepsilon_{\text{C-GYR}} t \\ \theta_{\text{ARW}} = \dfrac{1}{60}\sqrt{p_{\text{PSD}}} \\ \theta_{\text{BRW}} = \dfrac{\theta_{\text{BS}}}{\sqrt{t}} \\ \theta_{\text{TE}} = f(T) \end{cases} \tag{1}$$

where $\theta_C\ (t)$ is the linear angular error with time of rate gyros, $\varepsilon_{\text{C-GYR}}$ represents the constant error (°/h) or the inherent error, t denotes the time (s), θ_{ARW} is angle random walk caused by thermo-mechanical white noise, p_{PSD} is the power spectral density ((°/h)^2/Hz), θ_{BRW} is bias random walk caused by flicker noise (°/sqrt(h)), θ_{BS} is bias stability (°/h), and θ_{TE} is the bias effect of temperature on MEMS sensors

$$\begin{cases} s_C(t) = \varepsilon_{\text{C-ACC}} \dfrac{t^2}{2} \\ s_{\text{SD}} = \sigma \cdot t^{\frac{3}{2}} \cdot \sqrt{\dfrac{\delta t}{3}} \\ s_{\text{BRW}} \propto \dfrac{1}{\sqrt{t^5}} \\ s_{\text{TE}} = f(T) \end{cases} \tag{2}$$

where $s_C(t)$ is the linear angular error of the rate gyro, $\varepsilon_{\text{C-ACC}}$ is the constant bias error (m) or the inherent error, s_{SD} (m) is a standard deviation (Std) of a second-order random walk in position caused by accelerometer white noise, δt is the time interval between successive samples, s_{BRW} is the bias random walk due to flicker noise, and s_{TE} denotes the nonlinear bias effect of temperature.

The MEMS-INS error equations are derived as follows, with the east-north-upward geographic coordinate system as the navigation frame (n-frame) and the right-forward-upward as the body frame (b-frame) [3]:

$$\dot{\boldsymbol{\psi}}^n = \delta\omega_{ie}^n + \delta\omega_{en}^n - \left(\omega_{ie}^n + \omega_{en}^n\right) \times \boldsymbol{\psi}^n - \zeta^n + \delta\theta \tag{3}$$

$$\delta\dot{\boldsymbol{V}}^n = \boldsymbol{f}^n \times \boldsymbol{\psi}^n - \left(2\delta\omega_{ie}^n + \delta\omega_{en}^n\right) \times \boldsymbol{V}^n - \left(2\omega_{ie}^n + \omega_{en}^n\right) \times \delta\boldsymbol{V}^n + \gamma^n + \delta s \tag{4}$$

$$\begin{pmatrix} \delta\dot{L} \\ \delta\dot{\lambda} \\ \delta\dot{h} \end{pmatrix} = \begin{pmatrix} 0 & \dfrac{1}{R_M + h} & 0 \\ \dfrac{\sec L}{R_N + h} & 0 & 0 \\ 0 & 0 & 1 \end{pmatrix} \begin{pmatrix} \delta V_E \\ \delta V_N \\ \delta V_U \end{pmatrix} + \begin{pmatrix} 0 & \dfrac{V_N}{(R_M + h)^2} \\ \dfrac{V_E \sec L \cdot \tan L}{R_N + h} & -\dfrac{V_E \sec L}{(R_N + h)^2} \\ 0 & 0 \end{pmatrix} \begin{pmatrix} \delta L \\ \delta h \end{pmatrix} \tag{5}$$

where $\boldsymbol{\psi}^n = [\psi_E,\ \psi_N,\ \psi_U]^{\text{T}}$ is the attitude error vector; ω_{ie}^n and $\delta\omega_{ie}^n$ are the angular rate vector and its error due to rotation of the earth; ω_{ie}^n and $\delta\omega_{ie}^n$ are the angular rate vector and its error vector of the navigation frame relative to the earth; ζ^n is the gyroscope drift vector; $\delta\boldsymbol{V}^n = [\delta V_E,\ \delta V_N,\ \delta V_U\ ]$ is the velocity error vector; $\boldsymbol{f}^n$ is the specific force vector; γ^n is the accelerometers' bias in the n-frame; $\delta\theta$ and δs are the errors caused by rate gyroscope and accelerometer; L, λ, and h represent latitude, longitude, and altitude, respectively; δL, $\delta\lambda$, and δh denote their corresponding errors; and R_N and R_M are the radii of curvature in meridian and prime vertical, separately.

B. Improved Extended Kalman Filter

The MEMS-INS error is highly nonlinear due to IMU interior temperature [23], frequent stop-and-go of vehicles [26], and so on. To deal with this error, we introduce an IEKF, based on the following state vector [5]:

$$\boldsymbol{X} = [\boldsymbol{\psi}, \delta\boldsymbol{V}, \boldsymbol{\delta}, \boldsymbol{\gamma}, \boldsymbol{\zeta}]^{\text{T}} \tag{6}$$

where $\boldsymbol{\Psi}$, $\boldsymbol{V}$, $\boldsymbol{\delta}$, $\boldsymbol{\gamma}$, and $\boldsymbol{\zeta}$ are given by

$$\begin{cases} \boldsymbol{\psi} = [\psi_E, \psi_N, \psi_U] \\ \delta\boldsymbol{V} = [\delta V_E, \delta V_N, \delta V_U] \\ \boldsymbol{\delta} = [\delta L, \delta\lambda, \delta h] \\ \boldsymbol{\gamma} = [\gamma_{bx}, \gamma_{by}, \gamma_{bz}] \\ \boldsymbol{\zeta} = [\zeta_{bx}, \zeta_{by}, \zeta_{bz}] \end{cases} \tag{7}$$

with γ_{bx}, γ_{by}, and γ_{bz} and ζ_{bx}, ζ_{by}, and ζ_{bz} being the accelerometers' biases and gyroscopes drifts in b-frame, respectively. The IEKF for INS/GPS integration is given as below

$$\begin{cases} \boldsymbol{X}_k = f_k(\boldsymbol{X}_{k-1}) + \boldsymbol{V}_{k-1} \\ \boldsymbol{Z}_k = h_k(\boldsymbol{X}_k) + \boldsymbol{W}_k \end{cases} \tag{8}$$

where f_k and h_k denote the nonlinear functions of transition and observation processes, $\boldsymbol{V}_k$ and $\boldsymbol{W}_k$ are independent system and measurement noises vectors with covariance $\boldsymbol{Q}_k$ and $\boldsymbol{R}_k$, respectively, and $\boldsymbol{Z}_k$ is the measurement vector subtracting GPS measurement from the INS data. The IEKF algorithm is divided into the following two steps.

1) Time Update: a priori state is computed together with the state transition Jacobian, which is used to evaluate the predicted covariance

$$\hat{\boldsymbol{X}}_{k,k-1} = f_{k-1}(\boldsymbol{X}_{k-1}), \quad \boldsymbol{F}_{k,k-1} \approx \frac{\partial f_k}{\partial X}\Big|_{X_{k-1}} \tag{9}$$

$$\boldsymbol{P}_{k,k-1} = \boldsymbol{F}_{k,k-1}\boldsymbol{P}_{k-1}\boldsymbol{F}_{k,k-1}^T + \boldsymbol{Q}_{k-1}. \tag{10}$$

2) Measurement Update: Observation Jacobian and Kalman filter gains are computed; *a priori* estimates are combined to provide *a posteriori* state and covariance estimates

$$\boldsymbol{H}_k \approx \frac{\partial h_k}{\partial X}\Big|_{\hat{X}_{k,k-1}}, \quad \boldsymbol{K}_k = \boldsymbol{P}_{k,k-1}\boldsymbol{H}_k^T\left(\boldsymbol{H}_k\boldsymbol{P}_{k,k-1}\boldsymbol{H}_k^T + \boldsymbol{R}_k\right)^{-1} \tag{11}$$

$$\hat{\boldsymbol{X}}_k = \hat{\boldsymbol{X}}_{k,k-1} + \boldsymbol{K}_k(Z_k - h_k\hat{\boldsymbol{X}}_{k,k-1}) \tag{12}$$

$$\boldsymbol{P}_k = \boldsymbol{P}_{k,k-1} - \boldsymbol{K}_k\boldsymbol{H}_k\boldsymbol{P}_{k,k-1} \tag{13}$$

where $\hat{\boldsymbol{X}}_{k,k-1}$ represents *a priori* estimate of the state vector, $\boldsymbol{P}_{k,k-1}$ is *a priori* estimate error covariance matrix, $\boldsymbol{P}_{k-1}$ is *a posteriori* estimate error covariance matrix, and $\boldsymbol{Q}_{k-1}$ is the process noise covariance matrix.

The IEKF assumes approximate equality of the estimated states in two consecutive time steps. The state prediction and update propagate through the nonlinear system functions, and the state and observation errors propagate through a separate linearized system, which is formulated as Taylor series of the estimate [30]–[33].

Due to the system noise in the fusion framework, there may be a certain error between the estimation of the IEKF and the actual state [13]. To obtain an accurate estimate, it is necessary to compare and adjust the information detected by the sensors. Let the state estimation at instant k be

$$o_k = \hat{\boldsymbol{X}}_k - f_{k,k-1}\boldsymbol{X}_{k-1}. \tag{14}$$

The error of state estimation at instant k can be obtained as

$$v_k = h_k\hat{\boldsymbol{X}}_k - \boldsymbol{Z}_k. \tag{15}$$

An adaptive adjustment procedure is involved for tuning the observed parameters in the system state

$$\begin{cases} e_k = -\boldsymbol{P}_k \cdot \eta_k \\ e_{\boldsymbol{X}_k} = \dfrac{1}{\alpha_k}\boldsymbol{P}_{\boldsymbol{X}_k}h_k \cdot \eta_k \end{cases} \tag{16}$$

where η_k is Lagrange multiplier vector, and the adaptive adjustment factor α_k is given by

$$\alpha_k = \begin{cases} 1, & |\Delta e_k| \le \beta_0 \\ \dfrac{\beta_0}{|\Delta e_k|}\left(\dfrac{\beta_1 - |\Delta e_k|}{\beta_1 - \beta_0}\right), & \beta_0 < |\Delta e_k| \le \beta_1 \\ 0, & \beta_1 < |\Delta e_k| \end{cases} \tag{17}$$

where β_0 and β_1 are constants.

In the IEKF algorithm, we assume that both the prediction and correction obey normal distribution. Then, the Taylor expansion is approximately given by

$$\boldsymbol{X}_k = f_{k-1}(\hat{\boldsymbol{X}}_{k-1}) + \boldsymbol{A}_{k-1}\boldsymbol{X}_{k-1} + \boldsymbol{B}_{k-1}\boldsymbol{V}_{k-1} \tag{18}$$

$$\boldsymbol{Z}_k = h_{k-1}(\hat{\boldsymbol{X}}_{k-1}) + \boldsymbol{C}_k\boldsymbol{X}_{k,k-1} + \boldsymbol{D}_k\boldsymbol{W}_k \tag{19}$$

where $\boldsymbol{A}_{k-1}$, $\boldsymbol{B}_{k-1}$, $\boldsymbol{C}_k$, and $\boldsymbol{D}_k$ are Jacobian matrices, which can be obtained by

$$\boldsymbol{A}_{k-1} \approx \frac{\partial f_{k-1}}{\partial \hat{\boldsymbol{X}}_{k-1}} = \frac{\partial f(\boldsymbol{X}_{k-1}, \boldsymbol{V}_{k-1})}{\partial \boldsymbol{X}_{k-1}}\Big|_{(\boldsymbol{X}_{k-1}, \boldsymbol{V}_{k-1}) = (\hat{\boldsymbol{X}}_{k-1}, 0)} \tag{20}$$

$$\boldsymbol{B}_{k-1} \approx \frac{\partial f_{k-1}}{\partial \hat{\boldsymbol{V}}_{k-1}} = \frac{\partial f(\boldsymbol{X}_{k-1}, \boldsymbol{V}_{k-1})}{\partial \boldsymbol{V}_{k-1}}\Big|_{(\boldsymbol{X}_{k-1}, \boldsymbol{V}_{k-1}) = (\hat{\boldsymbol{X}}_{k-1}, 0)} \tag{21}$$

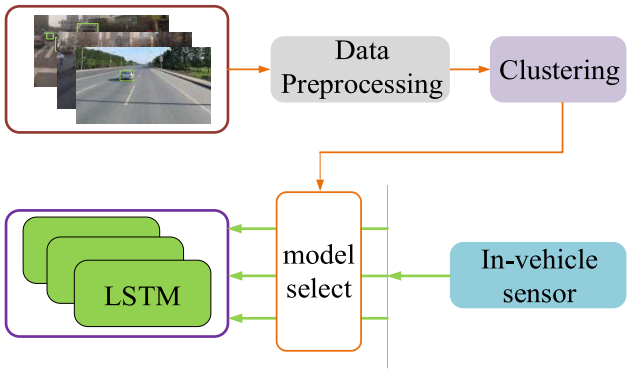

Fig. 2. Environment identification framework.

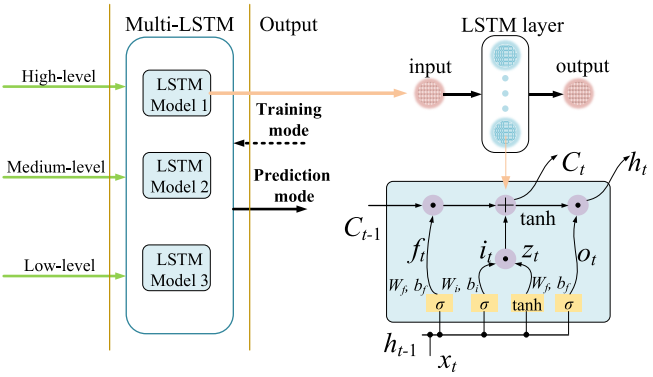

Fig. 3. Overall architecture of multi-LSTM network.

$$\boldsymbol{C}_k \approx \frac{\partial h_k}{\partial \hat{\boldsymbol{X}}_{k,k-1}} = \frac{\partial h(\boldsymbol{X}_k, \boldsymbol{W}_k)}{\partial \boldsymbol{X}_k}\Big|_{(\boldsymbol{X}_k, \boldsymbol{W}_k) = (\hat{\boldsymbol{X}}_{k,k-1}, 0)} \tag{22}$$

$$\boldsymbol{D}_k \approx \frac{\partial h_k}{\partial \hat{\boldsymbol{W}}_{k,k-1}} = \frac{\partial h(\boldsymbol{X}_k, \boldsymbol{W}_k)}{\partial \boldsymbol{W}_k}\Big|_{(\boldsymbol{X}_k, \boldsymbol{W}_k) = (\hat{\boldsymbol{X}}_{k,k-1}, 0)}. \tag{23}$$

In the prediction phase of IEKF algorithm, the gain formulation is the same as (11), and the error covariance matrix $\boldsymbol{P}_{k,k-1}$ is updated by

$$\boldsymbol{P}_{k,k-1} = \boldsymbol{A}_{k-1}\boldsymbol{P}_{k-1}\boldsymbol{A}_{k-1}^T + \boldsymbol{B}_{k-1}\boldsymbol{D}_{k-1}\boldsymbol{B}_{k-1}^T \tag{24}$$

and the error correction is performed via

$$\tilde{\boldsymbol{e}}_k = e_k\boldsymbol{Z}_k\boldsymbol{X}_{k,k-1}. \tag{25}$$

Finally, the state prediction equation is expressed as

$$\boldsymbol{X}_k = \boldsymbol{X}_{k,k-1} + \boldsymbol{K}_k\tilde{\boldsymbol{e}}_k. \tag{26}$$

C. Multi-LSTM Model

LSTM can deal with vanishing gradient and exploding gradient that cannot be handled by traditional neural networks [34]. However, it is infeasible to use a single LSTM model under all circumstances in complex and changeable driving environments. To deal with variable driving conditions, here we introduce a multi-LSTM architecture (as shown in Fig. 2) with three different LSTM networks, each of which has an independent learning engine and is used for position estimation in a certain traffic scenario it is trained for.

In what follows, we describe how the multi-LSTM framework is designed and how it is trained and used for prediction in different environments. The correlation between the interconnected time series of the images from the camera is extracted, by which the driving scenarios are divided into different categories with high, medium, and low complexity (see Fig. 3). Denote the selected feature vector as y_i, whose probability distribution is approximated using the GMM corresponding to different clustering sets with centers m as

$$p(y) = \sum_{1}^{m} p(m)p(y|m) = \sum_{1}^{m} \pi_m N(y|\mu_m, \Sigma_m) \quad (27)$$

where $N(y|\mu_m, \Sigma_m)$ is the mth component of the GMM with parameters $\{\mu_m, \Sigma_m\}$ and $p(m)$ is the weight of the mth Gaussian model. The category of the driving environment is determined by the posterior probability $p(m|x)$.

Next, by (27), the probability distributions are calculated from different traffic scenarios images collected in advance and stored with different classes (low, medium, and high complexity) in the model. Then, the traffic scene can be determined by comparing the current and the stored probability distributions, which is done based on the KL distance [35]. Denote the GMM for the current traffic image by p, and those for the low, medium, and high complexity images' classes by p^1_{class} , p^2_{class}, and p^3_{class}, respectively. Then, the KL distance is given as below

$$d_i\left(p \parallel p^i_{\text{class}}\right) = E_p \log \frac{p}{p^i_{\text{class}}}, \quad (i = 1, 2, 3) \quad (28)$$

where d_i is the KL distance, E_p is the expected value function, and i is the number of classes of the traffic environment. The current driving scenario can be determined by the case with the minimum distance.

The LSTM model can achieve accurate vehicle positioning in different scenarios since LSTM modules are capable of selectively remembering long-term information by taking advantage of feedback from the cycle unit. The loop unit in the LSTM contains three gate functions, including input gate i, forget gate f, and output gate o [25], [34]. The forget gate f determines what information from the previous state will be forgotten, which is described by

$$f_t = \sigma(W_f x_t + U_f h_{t-1} + b_f). \quad (29)$$

The input gate determines whether or not to add data from input information to the previous state, and it is expressed as below

$$i_t = \sigma(W_i x_t + U_i h_{t-1} + b_i) \quad (30)$$

$$z_t = \tanh(W_z x_t + U_z h_{t-1} + b_z) \quad (31)$$

$$c_t = f_t \odot c_{t-1} + i_t \odot z_t. \quad (32)$$

The output gate determines which information be maintained in the next hidden state, and it is given by

$$o_t = \sigma(W_o x_t + U_o h_{t-1} + b_o) \quad (33)$$

$$h_t = o_t \odot \tanh(c_t) \quad (34)$$

where x is the input data at time t, h represents the hidden state, c denotes the previous cell state, z is used to modify the cell state, W and U are the weights, b is a bias, and $\odot$ represents the Hadamard product.

Based on the above discussions, we now give the following pseudo algorithm for vehicle position estimation during GPS outages.

Algorithm 1 Vehicle Position Estimation During GPS Outages

Input:
Vehicle information based on GPS, MEMS-INS and in-vehicle sensors.
Output:
Position prediction information.

Procedure Model Predicting
  for starting criteria is met **do**
    Initialization of $\{\Psi, V, \delta, \gamma$ and $\zeta\}$ and initial position P_{C0}
    Compute p using (27)
    According to (28), compute d_i, $i \in \{1,2,3\}$
    $i \leftarrow \min\{d_i\}$
    output the predicted value ΔP_C with LSTM model i
    measurement $\leftarrow P_{C0} + \sum \Delta P_C$
    Calculate $\boldsymbol{P}_k$ according to (13)
    Calculate adaptive adjustment factor α_k according to (17)
    Predict the state according to (26)
  end for
repeat
until stopping criteria is met
end procedure

It is worth mentioning that, by introducing an IEKF filter to deal with noises in MEMS and using a multi-LSTM model with Gaussian mixture mechanism for classifying the environments to improve algorithm adaptability, our method is more accurate than the state-of-the-art methods in position estimation during GPS outage. To name a few, the Kalman filter-based method in [4] considers both noises of MEMS and GPS outages, but the estimate is not accurate enough. The zero-velocity detection scheme in [26] can deal with stopping events or high-frequency vehicle stops, but cannot give effective estimate of the vehicle position when GPS outages occur.

IV. Performance Evaluation

A. Numerical Simulations

In the experiment, the sample contains five inputs, i.e., wheel speed, steering angle, angular rate, specific force, and temperature inside IMU. Under a medium traffic condition, there are 13 time steps each with a feature length 5. In each time step, the intermediate vector of the LSTM has a dimension 10, so the number of input data is 130. The number of neurons in the forget gate layer is $N_{s1} = 160$, which can be calculated by (29), with the length of $(W_f h_{t-1} + U_f x_t)$ be 15, the length of the hidden vector be 10, and the length of offset b_f be 10. The number of neurons in the input gate can be calculated similarly as $N_{s2} = 320$. Also, we can get the number of neurons in the output gate according to (33) and (34) to be $N_{s3} = 160$. Summing-up N_{s1}, N_{s2}, and N_{s3} is the total number of neurons, namely, 640. The number of unrolls to be performed is 100. The sensor parameters in the simulations are shown in Table I.

We first show the performance of our method via numerical simulations performed in a vehicle driving situation with a circular trajectory whose radius is 8 m.

TABLE I
SENSORS' SPECIFICATIONS OF SIMULATION

Sensors	Parameters	Accuracy
IMU	Sample Rate	100Hz
	Temperature	25℃
	Gyro angle random walk	(rad/s)*√Hz
	Gyro bias stability in-run	< 70°/h
	ACC velocity random walk	(m/s²)*√Hz
	ACC bias stability in-run	0.25mg
GPS	Update Rate	10Hz
	Velocity accuracy	0.1m/s
	Horizontal Position Accuracy	1.6m
	Vertical Position Accuracy	3m

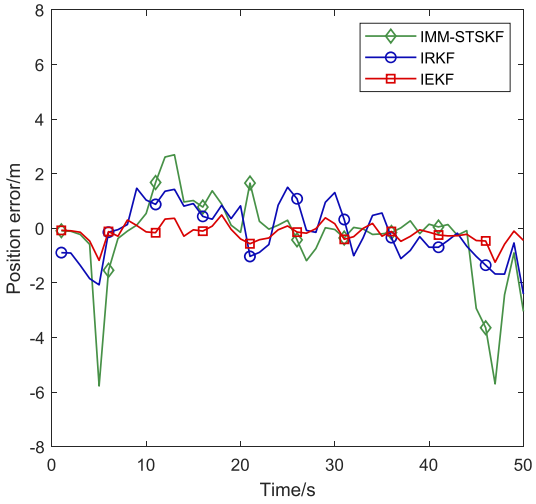

Fig. 4. Position error comparison results of IMM-STSKF, IRKF, and IEKF.

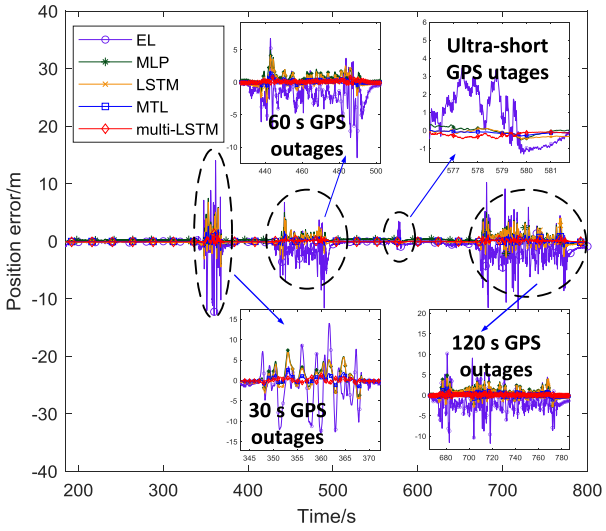

Fig. 5. Comparisons of position prediction errors during GPS outages of different algorithms in the simulation.

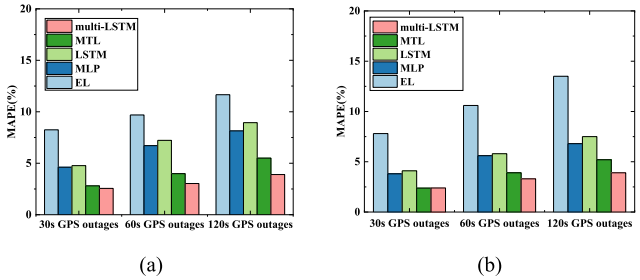

Fig. 6. Performance comparison of different predictors in terms of MAPE of vehicle position prediction during GPS outages. (a) Latitude. (b) Longitude.

To verify the effectiveness of the proposed IEKF algorithm, we first maintain the validity of the GPS sensor. Fig. 4 shows the position errors of our IEKF in comparison with two state-of-the-art methods of interacting multiple model-based sequential two-stage Kalman filter (IMM-STSKF) in [4] and innovation-based robust Kalman filter (IRKF) in [5] in a driving scene with frequent start–stop. The mean square errors of these three methods are 0.56, 2.69, and 1.03 m, respectively, which mean a reduction of the positioning error by 79.18% and 45.63% on average. The result shows that the IEKF method is advantageous for position estimation, which is because the use of adaptive correction reduces the influence of errors and avoids model dependence.

Comparisons for vehicle localization during GPS outages are also conducted between the ensemble learning algorithm (EL) in [23], multiple layer perceptron (MLP) in [24], LSTM in [25], and multi-task learning (MTL) in [26]. In the simulations, we considered three cases of GPS outages, i.e., short-time, medium-time, and long-time GPS failures, with 30-, 60-, and 120-s outages, respectively. The simulation results are shown in Fig. 5, from which it is clear that the proposed multi-LSTM can provide more accurate positioning during GPS outages in most cases. In particular, the multi-LSTM model shows stable output during very short GPS outages (less than 5 s), implying satisfactory fault-tolerant ability.

Further comparisons are made based on the mean absolute percentage error metric defined below

$$\text{MAPE} = \frac{1}{N}\sum_{n=1}^{N}\left|\frac{M_n(X_n) - M_n^p(X_n)}{M_n(X_n)}\right| \times 100$$

where $M_n(X_n)$ is the actual measurement value in state X_n, $M_n^p(X_n)$ is the predicted one, and N is the prediction times.

The comparisons are shown in Fig. 6, from which we can see that the proposed multi-LSTM method has the lowest MAPE and is effective to predict the vehicle position in both long and short complete GPS outages with high confidence. During GPS outage with duration of 120 s, in comparison with the four existing methods, the latitudinal MAPE reduces by 66.55%, 52.13%, 56.39%, and 29.09%, respectively, while the longitudinal MAPE reduces by 71.11%, 42.65%, 48.62%, and 25.06%, respectively.

Also, to verify the adaption of our proposed method in changeable urban environments, comparisons are made between the cases of MTL [26] and multi-LSTM under different environments (see Fig. 7). In this simulation, we try to simulate the real urban driving state and set three different scenes with various simulated noises. It is seen that the

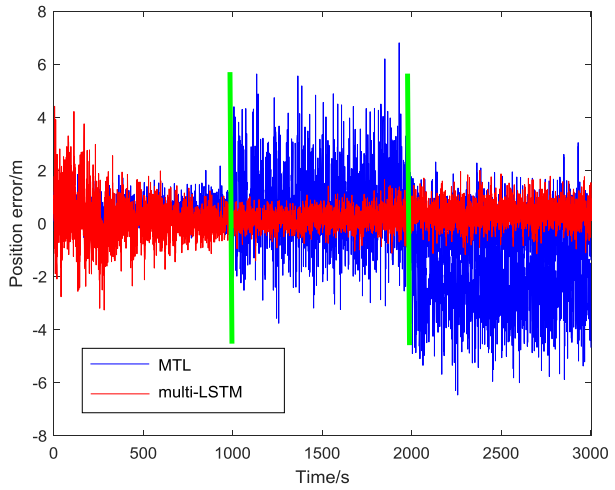

Fig. 7. MTL versus multi-LSTM under different environments.

MTL model cannot adapt to different environments and yield large prediction errors, while the multi-LSTM model provides accurate prediction under changeable environments.

B. Road Tests

Real road tests were performed to verify the proposed method. The sampling frequencies of the low-cost MEMS-based IMU and the GPS receiver are 100 and 10 Hz, respectively. The measurements of the wheel speed sensor and the steering sensor are collected from the CAN bus. The traffic scene is collected with 36-m length (W) and 24-m width (H) at a distance of 50 m (D). So the field of view (FOV) can be calculated as follows:

$$\begin{cases} \alpha_h = 2\arctan\left(\dfrac{W/2}{D}\right) \approx 36.4^\circ \\ \alpha_v = 2\arctan\left(\dfrac{H/2}{D}\right) \approx 26.9^\circ \\ \alpha_d = 2\arctan\left(\dfrac{\sqrt{W^2+H^2}/2}{D}\right) \approx 46.7^\circ. \end{cases}$$

Then, using the camera parameters such as focal length f, image specification v^*h, and diagonal d, we can get that

$$\alpha_h = 2\arctan\frac{h}{2f}, \quad \alpha_v = 2\arctan\frac{v}{2f}$$
$$\alpha_d = 2\arctan\frac{d}{2f} d^2 = h^2 + v^2.$$

Therefore, it can be calculated from the FOV formula that $f \approx 50$ mm, image size 24 mm * 36 mm, and $d \approx 43$ mm. Therefore, we use a high-definition camera GT-1408 from MIGNOVA Company Ltd., which is placed in the front of the vehicle. The specifications of the sensors are given in Table II.

The performance of the proposed method was tested with real-world data collected using IMU, KT700, and an HD camera (GT-1408) on a 20-km urban road in Shenyang with dense traffic for about 55 min. Moreover, the experiments

TABLE II
SENSORS' SPECIFICATIONS

Sensors	Parameters	Accuracy
IMU	Sample Rate	100Hz
	ACC velocity random walk	0.08 m/s/√h
	ACC bias stability in-run	0.25mg
	Gyro angular random walk	0.2°/√h
	Gyro bias stability	< 70°/h
	Temperature	25℃
GPS	Update Rate	10Hz
	Horizontal Position Accuracy	1.6m
	Vertical Position Accuracy	3m
HD Camera	Pixel	2 million
	Resolution	1280*720
In-vehicle sensors data collector (KT700)	input voltage	DC7-32V
	power	<5W
	RJ45 network interface	10/100M

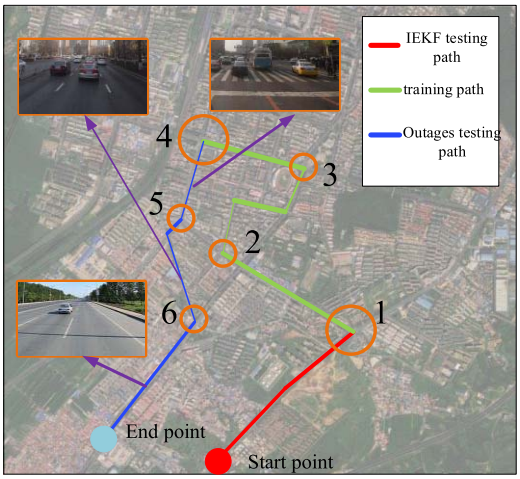

Fig. 8. Trajectory of the road experiment.

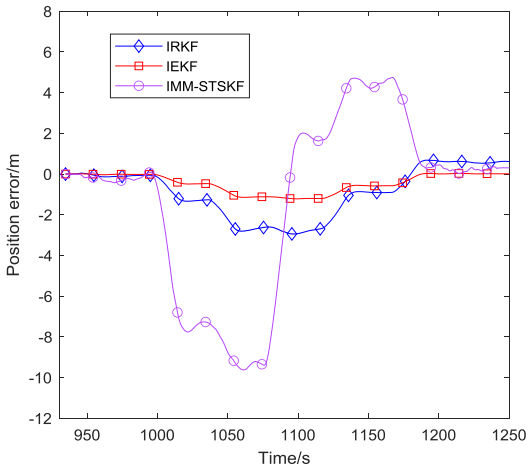

Fig. 9. Results comparing with IMM-STSKF and IRKF.

involved three different urban trajectories (see Fig. 8). Trajectory one (5 min) with red color is to verify the proposed IEKF algorithm. The training tests (25 min) and prediction tests (25 min) are verified, respectively, in trajectory two with green color and trajectory three with blue color, for high

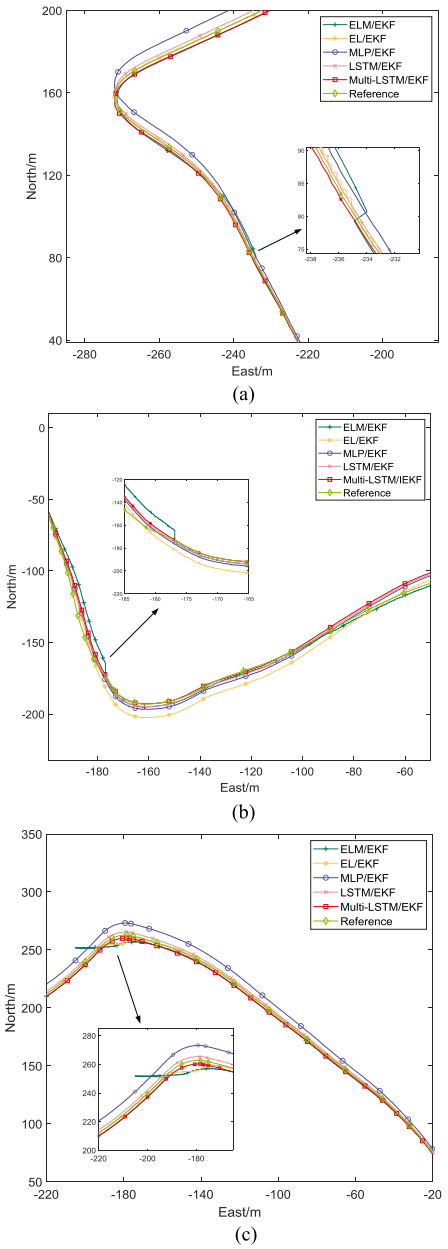

Fig. 10. Different environmental complexity trajectory during GPS outages. (a) Low complexity trajectory. (b) Medium complexity trajectory. (c) High complexity trajectory.

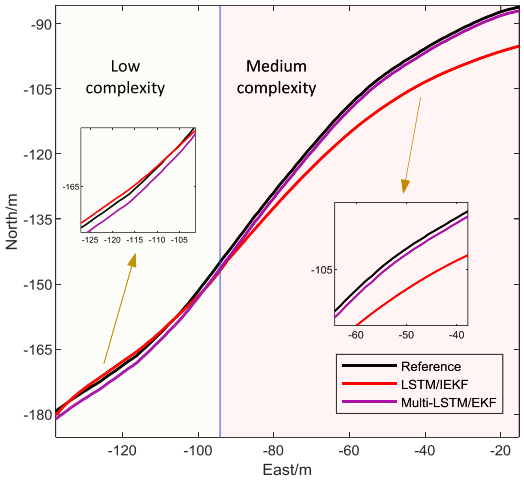

Fig. 11. Comparison of combinations LSTM/IEKF and multi-LSTM/EKF.

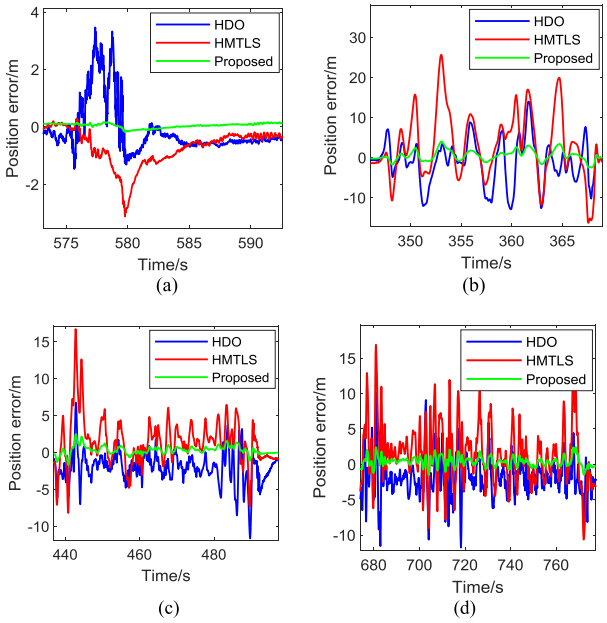

Fig. 12. Comparison of position errors of different algorithms. (a) Ultrashort GPS outage. (b) 30-s GPS outage. (c) 60-s GPS outage. (d) 120-s GPS outage.

(point 1 to 2, point 4 to 5), medium (point 2 to 3, point 5 to 6), and low (point 3 to 4, point 6 to end) complexity cases.

To verify the effectiveness of the proposed IEKF algorithm, a comparison experiment was done with IMM-STSKF [4] and IRKF [5] in trajectory one (see Fig. 9). It is clear that the proposed algorithm can improve positioning accuracy effectively.

The performance of the multi-LSTM model during GPS outages is verified by comparison in invariant environments with manual removal of GPS. The results are shown in Fig. 10, where (a) gives the comparison of low complexity and (b) and (c) are for medium and high complexity, respectively. Here, we consider four different combinations for comparison [4], [23]–[25], namely extreme learning machine/EKF (ELM/EKF), EL/EKF, MLP/EKF, and LSTM/EKF. It is seen that our multi-LSTM method can provide more accurate position prediction than other methods.

To evaluate the significance of multi-LSTM and IEKF on the accuracy of position prediction, we show the performances of two other combinations of multi-LSTM/EKF and LSTM/IEKF in Fig. 11 using AI models trained in advance. We can find that the position drift of model LSTM/IEKF is less than that of model multi-LSTM/EKF under invariable road conditions (see left side in the figure). While under changing traffic conditions, the position prediction of model LSTM/IEKF severely shifted over time (see right side of the figure). We can conclude that IEKF is more significant under invariable road conditions (low complexity level), while multi-LSTM plays a more important role under changing road conditions (high complexity level).

Fig. 12 shows the comparisons of the proposed model with the state-of-the-art results of hybrid dual optimization (HDO) [24] and heterogeneous multi-task learning system (HMTLS)

TABLE III
STD AND RMSE OF POSITION ERRORS WITH DIFFERENT ADVANCED METHODS

methods	Outages time	Std	RMSE
HDO	ultra-short	1.27	2.47
	30s	1.31	3.86
	60s	1.82	11.27
	120s	1.97	18.62
HMTL	ultra-short	1.24	2.28
	30s	1.37	2.93
	60s	1.62	6.54
	120s	1.69	10.87
Proposed method	ultra-short	0.11	1.15
	30s	0.12	2.69
	60s	0.13	2.34
	120s	0.15	3.08

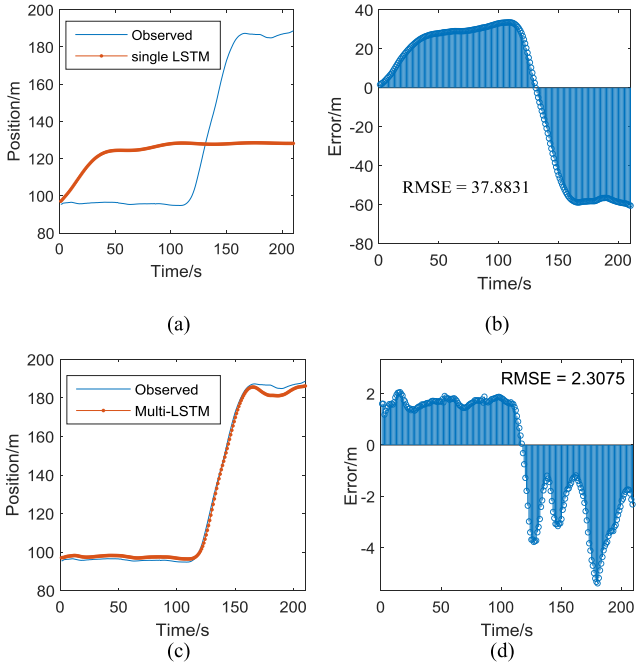

Fig. 13. Prediction result and RMSE of single LSTM and multi-LSTM in changing environments. (a) Prediction result of single LSTM. (b) Errors of single LSTM. (c) Prediction result multi-LSTM. (d) Errors of multi-LSTM.

architecture [26]. Table III summarizes the Std and the root-mean-square error (RMSE) defined below of position prediction during GPS outages with different durations

$$\mathrm{RMSE} = \sqrt{\frac{1}{N}\sum_{n=1}^{N}\left(M_n^p(X_n) - M_n(X_n)\right)^2}$$

where $M_n(X_n)$ is the actual measurement in state X_n, $M_n^p(X_n)$ is the predicted one, and N is the prediction times.

From Fig. 12, we can find that our method is superior to the others in stability and accuracy. Especially, it is worth noting that our method can effectively handle GPS ultrashort outages that cannot be dealt with by the other methods. Moreover, the Std and RMSE of north position, respectively, reduce by 53.1% and 50.2%, 30.3% and 8%, 78% and 64%, and 83% and 71% during ultrashort, 30-, 60-, and 120-s GPS outages (see Table III). The reason why the proposed method provides stable and accurate localization is that the estimation ability

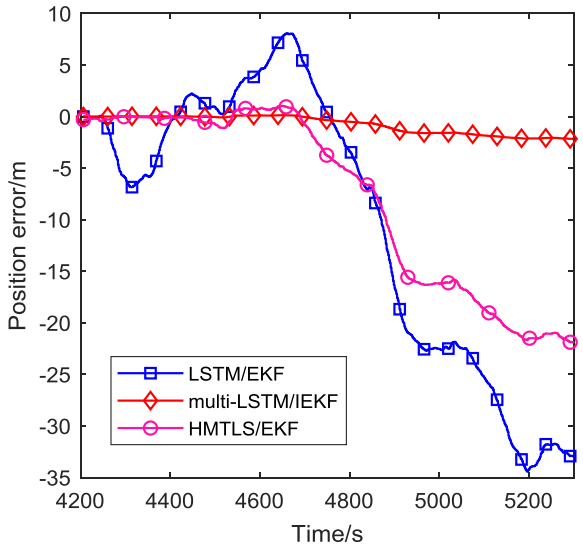

Fig. 14. Comparison of the performance of single LSTM mode and multi-LSTM mode in different urban environments.

of IEKF can optimize the output, and the predictive ability of multi-LSTM can elaborate the predicted values.

In order to verify that our method (see Algorithm 1) can provide stable position estimation in changeable urban environment during GPS outages, further comparison experiments are conducted in trajectory three including our multi-LSTM/IEKF, LSTM/EKF model in [25], and HMTLS/EKF model in [26] to verify the adaptability of our method in changing driving environments (see Figs. 13 and 14). It is clear that the multi-LSTM method performs better. In other words, the multi-LSTM model can adapt to changeable environments effectively and perform well in different environments with GPS outages for a long time, and the RMSE of position reduces by 93.9%.

V. CONCLUSION AND FUTURE WORK

In this article, a novel vehicle localization with adaptive IEKF and deep learning scheme is proposed to improve the position accuracy in variable urban environments during GPS outages. The adaptive IEKF is capable of handling inherent nonlinearity in the measurements and state, making the method more accurate, fault tolerant, and in dependence of the process model. The vision classification based on GMM and KL distance enables the IEKF and multi-LSTM model to activate the appropriate LSTM modules corresponding to the traffic scenes. In this way, the proposed method performs more accurately and reliably compared with the state-of-the-art methods for vehicle localization in changeable environments during GPS outages, with a reduction of the RMSE of positioning of 93.9%.

Our future research will focus on finding advanced fusion method based on multimodal MEMS/INS/GNSS sensors. Accurate cooperative vehicle localization via the use of vehicular *ad hoc* networks (VANETs) is also worth investigation in adverse environments.

REFERENCES

[1] L. Delobel, R. Aufrere, C. Debain, R. Chapuis, and T. Chateau, "A real-time map refinement method using a multi-sensor localization framework," *IEEE Trans. Intell. Transp. Syst.*, vol. 20, no. 5, pp. 1644–1658, May 2019.

[2] S. Kuutti, S. Fallah, K. Katsaros, M. Dianati, F. Mccullough, and A. Mouzakitis, "A survey of the state-of-the-art localization techniques and their potentials for autonomous vehicle applications," *IEEE Internet Things J.*, vol. 5, no. 2, pp. 829–846, Apr. 2018.

[3] E. Zhang and N. Masoud, "Increasing GPS localization accuracy with reinforcement learning," *IEEE Trans. Intell. Transp. Syst.*, vol. 22, no. 5, pp. 2615–2626, May 2021, doi: 10.1109/TITS.2020.2972409.

[4] Q. Xu, X. Li, and C.-Y. Chan, "Enhancing localization accuracy of MEMS-INS/GPS/in-vehicle sensors integration during GPS outages," *IEEE Trans. Instrum. Meas.*, vol. 67, no. 8, pp. 1966–1978, Aug. 2018.

[5] D. Wang, Y. Dong, Z. Li, Q. Li, and J. Wu, "Constrained MEMS-based GNSS/INS tightly coupled system with robust Kalman filter for accurate land vehicular navigation," *IEEE Trans. Instrum. Meas.*, vol. 69, no. 7, pp. 5138–5148, Jul. 2020.

[6] J. K. Suhr, J. Jang, D. Min, and H. G. Jung, "Sensor fusion-based low-cost vehicle localization system for complex urban environments," *IEEE Trans. Intell. Transp. Syst.*, vol. 18, no. 5, pp. 1078–1086, May 2017.

[7] Y. Gu, L.-T. Hsu, and S. Kamijo, "GNSS/onboard inertial sensor integration with the aid of 3-D building map for lane-level vehicle self-localization in urban canyon," *IEEE Trans. Veh. Technol.*, vol. 65, no. 6, pp. 4274–4287, Jun. 2016.

[8] S. Zhao, Y. Chen, and J. A. Farrell, "High-precision vehicle navigation in urban environments using an MEM's IMU and single-frequency GPS receiver," *IEEE Trans. Intell. Transp. Syst.*, vol. 17, no. 10, pp. 2854–2867, Oct. 2016.

[9] B. Renfro, J. Rosenquest, A. Terry, and N. Boeker, "An analysis of global positioning system (GPS) Standard positioning system (SPS) performance for 2014," Space Geophys. Lab., Appl. Res. Laboratories, Univ. TX Austin, Austin, TX, USA, Tech. Rep. TR-SGL-17-02, 2017.

[10] J. Farrell and M. Barth, *The Global Positioning System and Inertial Navigation*, vol. 61. New York, NY, USA: McGraw-Hill, 1999, pp. 113–123.

[11] A. Noureldin, T. B. Karamat, M. D. Eberts, and A. El-Shafie, "Performance enhancement of MEMS-based INS/GPS integration for low-cost navigation applications," *IEEE Trans. Veh. Technol.*, vol. 58, no. 3, pp. 1077–1096, Mar. 2009.

[12] K.-W. Chiang *et al.*, "Assessment for INS/GNSS/odometer/barometer integration in loosely-coupled and tightly-coupled scheme in a GNSS-degraded environment," *IEEE Sensors J.*, vol. 20, no. 6, pp. 3057–3069, Mar. 2020.

[13] M. Narasimhappa, A. D. Mahindrakar, V. C. Guizilini, M. H. Terra, and S. L. Sabat, "MEMS-based IMU drift minimization: Sage Husa adaptive robust Kalman filtering," *IEEE Sensors J.*, vol. 20, no. 1, pp. 250–260, Jan. 2020.

[14] L. Cong, S. Yue, H. Qin, B. Li, and J. Yao, "Implementation of a MEMS-based GNSS/INS integrated scheme using supported vector machine for land vehicle navigation," *IEEE Sensors J.*, vol. 20, no. 23, pp. 14423–14435, Dec. 2020.

[15] W. Guangcai, X. Xu, and T. Zhang, "M-M estimation-based robust cubature Kalman filter for INS/GPS integrated navigation system," *IEEE Trans. Instrum. Meas.*, vol. 70, 2021, Art. no. 9501511, doi: 10.1109/TIM.2020.3021224.

[16] B. Cui, X. Chen, X. Tang, H. Huang, and X. Liu, "Robust cubature Kalman filter for GNSS/INS with missing observations and colored measurement noise," *ISA Trans.*, vol. 72, pp. 138–146, Jan. 2018.

[17] Y. Yao, X. Xu, C. Zhu, and C.-Y. Chan, "A hybrid fusion algorithm for GPS/INS integration during GPS outages," *Measurement*, vol. 103, pp. 42–51, Jun. 2017.

[18] O. Kaiwartya *et al.*, "Geometry-based localization for GPS outage in vehicular cyber physical systems," *IEEE Trans. Veh. Technol.*, vol. 67, no. 5, pp. 3800–3812, May 2018.

[19] H. Qin, L. Cong, and X. Sun, "Accuracy improvement of GPS/MEMS-INS integrated navigation system during GPS signal outage for land vehicle navigation," *J. Syst. Eng. Electron.*, vol. 23, no. 2, pp. 256–264, Apr. 2012.

[20] L. Chen and J. Fang, "A hybrid prediction method for bridging GPS outages in high-precision POS application," *IEEE Trans. Instrum. Meas.*, vol. 63, no. 6, pp. 1656–1665, Jun. 2014.

[21] R. Sharaf, A. Noureldin, A. Osman, and N. El-Sheimy, "Online INS/GPS integration with a radial basis function neural network," *IEEE Aerosp. Electron. Syst. Mag.*, vol. 20, no. 3, pp. 8–14, Mar. 2005.

[22] Y. Huang, Z. Zhang, S. Du, Y. Li, and Y. Zhang, "A high-accuracy GPS-aided coarse alignment method for MEMS-based SINS," *IEEE Trans. Instrum. Meas.*, vol. 69, no. 10, pp. 7914–7932, Oct. 2020.

[23] J. Li, N. Song, G. Yang, M. Li, and Q. Cai, "Improving positioning accuracy of vehicular navigation system during GPS outages utilizing ensemble learning algorithm," *Inf. Fusion*, vol. 35, pp. 1–10, May 2017.

[24] C. Shen, Y. Zhang, J. Tang, H. Cao, and J. Liu, "Dual-optimization for a MEMS-INS/GPS system during GPS outages based on the cubature Kalman filter and neural networks," *Mech. Syst. Signal Process.*, vol. 133, Nov. 2019, Art. no. 106222.

[25] W. Fang *et al.*, "A LSTM algorithm estimating pseudo measurements for aiding INS during GNSS signal outages," *Remote Sens.*, vol. 12, no. 2, p. 256, Jan. 2020.

[26] S. Lu, Y. Gong, H. Luo, F. Zhao, Z. Li, and J. Jiang, "Heterogeneous multi-task learning for multiple pseudo-measurement estimation to bridge GPS outages," *IEEE Trans. Instrum. Meas.*, vol. 70, pp. 1–16, 2021, doi: 10.1109/TIM.2020.3028438.

[27] V. Havyarimana, D. Hanyurwimfura, P. Nsengiyumva, and Z. Xiao, "A novel hybrid approach based-SRG model for vehicle position prediction in multi-GPS outage conditions," *Inf. Fusion*, vol. 41, pp. 1–8, May 2018.

[28] S. Bijjahalli and R. Sabatini, "A high-integrity and low-cost navigation system for autonomous vehicles," *IEEE Trans. Intell. Transp. Syst.*, vol. 22, no. 1, pp. 356–369, Jan. 2021.

[29] H. Nourmohammadi and J. Keighobadi, "Decentralized INS/GNSS system with MEMS-grade inertial sensors using QR-factorized CKF," *IEEE Sensors J.*, vol. 17, no. 11, pp. 3278–3287, Jun. 2017.

[30] B. Feng, M. Fu, H. Ma, Y. Xia, and B. Wang, "Kalman filter with recursive covariance estimation—Sequentially estimating process noise covariance," *IEEE Trans. Ind. Electron.*, vol. 61, no. 11, pp. 6253–6263, Nov. 2014.

[31] F. Li and L. Chang, "MEKF with navigation frame attitude error parameterization for INS/GPS," *IEEE Sensors J.*, vol. 20, no. 3, pp. 1536–1549, Feb. 2020.

[32] M. Bai, Y. Huang, Y. Zhang, and G. Jia, "A novel progressive Gaussian approximate filter for tightly coupled GNSS/INS integration," *IEEE Trans. Instrum. Meas.*, vol. 69, no. 6, pp. 3493–3505, Jun. 2020.

[33] M. Ramezani and K. Khoshelham, "Vehicle positioning in GNSS-deprived urban areas by stereo visual-inertial odometry," *IEEE Trans. Intell. Vehicles*, vol. 3, no. 2, pp. 208–217, Jun. 2018.

[34] J. Ma, H. Liu, C. Peng, and T. Qiu, "Unauthorized broadcasting identification: A deep LSTM recurrent learning approach," *IEEE Trans. Instrum. Meas.*, vol. 69, no. 9, pp. 5981–5983, Sep. 2020.

[35] H. Greenspan and A. T. Pinhas, "Medical image categorization and retrieval for PACS using the GMM-KL framework," *IEEE Trans. Inf. Technol. Biomed.*, vol. 11, no. 2, pp. 190–202, Mar. 2007.

Jiageng Liu received the B.S. degree from Liaoning Technical University, Fuxin, China, in 2008, and the M.S. degree from the Liaoning University of Technology, Jinzhou, China, in 2013. He is currently pursuing the Ph.D. degree with the College of Information Science and Engineering, Northeastern University, Shenyang, China.

His research interests include vehicle localization, deep learning, and intelligent transportation systems.

Ge Guo (Senior Member, IEEE) received the B.S. and Ph.D. degrees from Northeastern University (NEU), Shenyang, China, in 1994 and 1998, respectively.

In 1999, he joined the Lanzhou University of Technology, Lanzhou, China, where he was the Director of the Institute of Intelligent Control and Robots and a Professor from 2004 to 2005. He was with Dalian Maritime University, Dalian, China, as a Professor till 2017. He is currently a Professor with NEU and the Dean of the School of Control Engineering, Northeastern University at Qinhuangdao, Qinhuangdao, China. His research interests include intelligent transportation systems and cyber-physical systems.

Prof. Guo was a recipient of the Chinese Association of Automation (CAA) Young Scientist Award in 2017. He is also an Associate Editor of several journals, e.g., IEEE TRANSACTIONS ON INTELLIGENT TRANSPORTATION SYSTEMS, IEEE TRANSACTIONS ON INTELLIGENT VEHICLES, *Information Sciences, IEEE Intelligent Transportation Systems Magazine*, and *Acta Automatica Sinica*. He was an Honoree of the New Century Excellent Talents in University, Ministry of Education, in 2004, and a Nominee for Gansu Top Ten Excellent Youths by the Gansu Provincial Government in 2005.